JGR Atmospheres

RESEARCH ARTICLE
10.1029/2019JD031140

Key Points:
- Transboundary particulate matter pollution episodes (EP) were mainly caused by surface high pressure, cold front, dust storm, or typhoons
- Vertical wind profiles show the different relationships between wind speed at various altitudes and surface particulate matter
- The maximum transport height extended from surface to about 2.0 km or even higher in superregional and regional transboundary EPs

Supporting Information:
- Supporting Information S1

Correspondence to:
S. H. L. Yim,
steveyim@cuhk.edu.hk

Citation:
Yang, Y., Yim, S. H. L., Haywood, J., Osborne, M., Chan, J. C. S., Zeng, Z., & Cheng, J. C. H. (2019). Characteristics of heavy particulate matter pollution events over Hong Kong and their relationships with vertical wind profiles using high-time-resolution Doppler lidar measurements. *Journal of Geophysical Research: Atmospheres*, *124*, 9609–9623. https://doi.org/10.1029/2019JD031140

Received 6 JUN 2019
Accepted 19 JUL 2019
Accepted article online 29 JUL 2019
Published online 26 AUG 2019

Author Contributions:
Conceptualization: Steve H.L. Yim
Formal analysis: Yuanjian Yang, Steve H.L. Yim, Jim Haywood, Martin Osborne, Zhaoliang Zeng
Funding acquisition: Steve H.L. Yim
Methodology: Yuanjian Yang, Steve H.L. Yim
Software: Yuanjian Yang, Jazz C.S. Chan, Jack C.H. Cheng
Supervision: Steve H.L. Yim
Validation: Yuanjian Yang, Steve H.L. Yim, Jazz C.S. Chan, Jack C.H. Cheng
Visualization: Jack C.H. Cheng
Writing - original draft: Yuanjian Yang, Steve H.L. Yim
Writing – review & editing: Yuanjian Yang, Jim Haywood, Martin Osborne, *(continued)*

Characteristics of Heavy Particulate Matter Pollution Events Over Hong Kong and Their Relationships With Vertical Wind Profiles Using High-Time-Resolution Doppler Lidar Measurements

Yuanjian Yang[1,2], Steve H.L. Yim[3,1,4], Jim Haywood[5,6], Martin Osborne[5,6], Jazz C.S. Chan[3], Zhaoliang Zeng[3], and Jack C.H. Cheng[3]

[1]Institute of Environment, Energy and Sustainability, The Chinese University of Hong Kong, Hong Kong, China, [2]School of Atmospheric Physics, Nanjing University of Information Science and Technology, Nanjing, China, [3]Department of Geography and Resource Management, The Chinese University of Hong Kong, Hong Kong, China, [4]Stanley Ho Big Data Decision Analytics Research Centre, The Chinese University of Hong Kong, Hong Kong, China, [5]Department of Mathematics, College of Engineering, Mathematics and Physical Science, University of Exeter, Exeter, UK, [6]Met Office, Exeter, UK

Abstract Previous studies have reported boundary layer features related to air pollution. However, few studies have comprehensively evaluated the characteristics and mechanisms of vertical wind in the formation and evolution of heavy particulate matter pollution episodes (EP) in Hong Kong. In this study, we analyzed the vertical characteristics of heavy particulate matter (PM) pollutions over Hong Kong and their relationships with vertical wind profiles using high-time-resolution Doppler lidar measurements and hourly meteorological and air quality observations. We identified nine EPs and show that the events were closely coupled to various vertical wind profiles in the planetary boundary layer (PBL). Our analysis suggests that strong vertical wind speed with wind shear at certain heights in the PBL had a positive correlation with surface PM during most superregional transboundary EPs. The maximum transport height extends from the surface to about 2.0 km or even higher; these transport heights differed among superregional and regional transboundary EPs. At peak surface pollution concentrations during the nine EPs, the surface PM_{10} had a significant negative correlation with PBL heights/mixing layer heights, while the averaged wind shear in the PBL was significantly positively correlated. These EPs with different mixing layer heights were mainly driven by different vertical wind shear conditions under various weather systems related to surface high pressure, cold fronts, dust storms, and typhoons. This work provides scientific evidence that surface PM pollutions were closely related to the characteristics of vertical profiles during the transboundary air pollutions.

1. Introduction

Particulate matter (PM) pollution not only damages the environment and affects climate but leads to adverse impacts on human health, especially in China (Gu et al., 2018; Li et al., 2016; Orru et al., 2017; Yim & Barrett, 2012; Wang et al., 2019). It has been well recognized that the formation of PM pollution episodes is mainly determined by air pollutant emissions and particular meteorological conditions in China, such as calm/weak wind, low planetary boundary layer (PBL)/mixing layer height, strong temperature inversion, high relative humidity, and related local- and large-scale atmospheric circulations (Cai et al., 2017; Guo et al., 2011, 2016; Li et al., 2017; Liang et al., 2017; Liu et al., 2015; Miao et al., 2015; Wang et al., 2012; Wang & Chen, 2016; Xing et al., 2017; Yang et al., 2018; Zheng et al., 2019). In addition to local PM pollution, transboundary particulate matter pollution is also a significant contributor to air pollution episodes which has therefore drawn much attention (Fan et al., 2013; Gu & Yim, 2016; Yim et al., 2019; Kang et al., 2019; Miao et al., 2017; Osborne et al., 2019; Qi et al., 2014; Qin et al., 2016). For instance, Hou et al. (2018) applied a state-of-the-art atmospheric model to estimate that local and transboundary air pollution contributed 27% and 73% of the region's fine PM, respectively, in the Pearl River Delta (PRD) region of China. The largest impacts from transboundary air pollution over PRD occurred in winter when northerly winds mainly prevailed.

Jazz C.S. Chan, Zhaoliang Zeng, Jack C. H. Cheng

Hong Kong, as a subtropical high population density coastal city located in the PRD region of southern China, is one of the three largest economic and high-emission zones in China. Understanding pollution episodes over Hong Kong is important owing to the high concentrations of PM experienced by a large population density. Previous studies reported that meteorological conditions for pollution episodes in Hong Kong vary in different seasons, such as northerly wind during winter monsoon, and large-scale descent associated with high-pressure systems with northerly winds related to summer typhoons (Chung et al., 1999; Liu & Chan, 2002; Louie et al., 2005; Zhang et al., 2014; Tong et al., 2018; Luo et al., 2018; Yim et al., 2019). Even though previous studies have reported the significant and unique associations between meteorological variables at higher altitudes and surface air quality (Tong et al., 2018; Yim et al., 2019), the characteristics of vertical wind with aerosol in the formation and evolution of PM pollution episodes are still unclear due to the lack of synchronous high-time-resolution vertical observations of wind and aerosol, and thus, more research is needed.

Ground-based light detection and ranging (lidar) is a useful instrument for monitoring the vertical structure of atmosphere at high temporal and spatial resolution, especially in the PBL (e.g.,Fan et al., 2019 ; Liu et al., 2013 ; Manninen et al., 2018 ; Osborne et al., 2019 ; Pearson et al., 2010 ; Qin et al., 2016 ; Su et al., 2018). In particular, ground-based Doppler lidars can be deployed to remotely monitor vertical and horizontal winds and mixing processes to identify aerosol transport in the lower level of the atmosphere and to explore dynamic features of the PBL (Barlow et al., 2011; Harvey et al., 2013; Manninen et al., 2018). For Hong Kong, previous studies mainly focused on vertical PM and their derived PBL or mixing layer heights using ground-based lidars with single assumed aerosol backscatter coefficients (He et al., 2008; Mok & Rudowicz, 2004; Su et al., 2017; Yang et al., 2013). It is however difficult to identify transboundary air pollution due to lack of local wind profiles. Therefore, the sources, paths, and heights of transboundary air pollution have yet to be fully understood or directly observed in Hong Kong.

Using high-time-resolution vertical aerosol backscatter coefficients and wind profiles derived by ground-based Doppler lidar data, real-time monitoring surface PM data, and ground and sounding meteorological data, we identified nine PM pollution episodes in Hong Kong from March 2017 to January 2019. We comprehensively analyzed the characteristics and mechanisms of the nine episodes and performed trajectory analysis using high-resolution reanalysis data. In section 2, the Doppler lidar and its operating specification, together with all the employed data, are described. Results are shown and discussed in section 3 and section 4, respectively. Finally, a conclusion is given in section 5.

2. Data and Method

2.1. Doppler Lidar Observation

The StreamLine Doppler Lidar from Halo Photonics used in this paper was located at Physical Geography Experimental Station of The Chinese University of Hong Kong (22.415N°, 114.212E°; Figure 1). The deployed lidar is a Halo Photonics 1.5-μm pulsed Doppler instrument that had previously been used for exploring the PBL in the tropical and midlatitude environments (Pearson et al., 2010; Barlow et al., 2011; Harvey et al., 2013; Manninen et al., 2018). The lidar system was conceived to meet the need for remote sensing of motion and backscatter in the atmosphere, where naturally occurring aerosols and clouds act as a distributed target that backscatter the transmitted pulses. Derived variables include wind profiles, backscatter coefficient (β), turbulence parameters, and cloud base measurements. The lidar was set up to optimize the retrieval resolution in the boundary layer up to around 3-km altitude and operated in velocity azimuth display with its scanner configured to take wind profiles every 10 min. The spatial and temporal resolutions are 30 m and 1 s, respectively, when operating in vertical stare mode for the intervening periods.

Prior to its operation, a colocation comparison test has been conducted to validate our lidar. In the test, two other nominally identical Doppler lidars, which are, respectively, setting up to Guangzhou and Zhuhai in the PRD region, were operated simultaneously at a same location. All the three lidars are new instruments so they have been calibrated by the lidar manufacturer. The collected data by the three lidars were compared to show that the data were consistent within the 95% confidence interval indicating a satisfactory manufacturer calibration. The data collection period for this study was from March 2017 to January 2019, except for several intermittent months of unscheduled lidar maintenance for repairing by Halo Photonics, and routine maintenance checks for the lidar includes cleaning and leveling checks. In addition to the hourly automatic

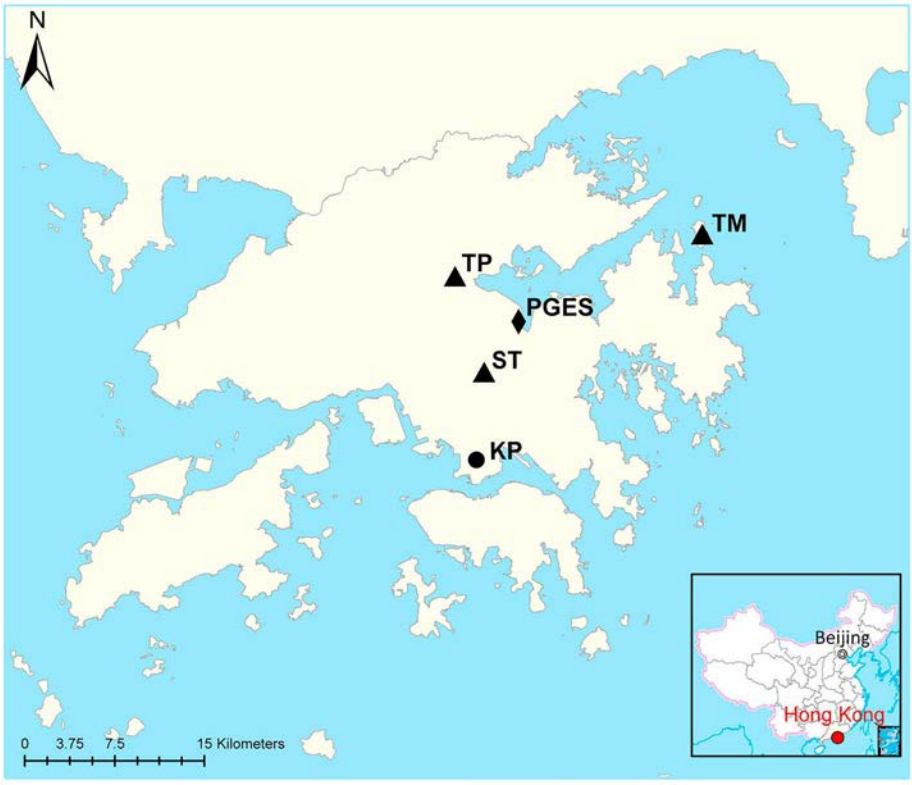

Figure 1. Map of Hong Kong with meteorological station, (KP) air quality stations [Tai Po (TP), Sha Tin (ST), Tap Mum (TM)] and our lidar at the Physical Geography Experimental Station (PGES) of The Chinese University of Hong Kong (CUHK).

wiping of the lidar window, deep cleaning was carried out at a frequency of a week where the windows were given a deep clean with an optical cleaning solution. Routine leveling checks were carried out at a frequency of a week to correct for any settling of the system into the ground surface. The precision of the leveling was within ±0.1°.

The performance of the Doppler measurement mainly depends on the detector noise of instrument and the natural atmospheric variability within the resolution volume (Päschke et al., 2015), with an optimal performance under high signal-noise ratio conditions. As suggested by Manninen et al. (2018), this study used a signal-noise ratio of −20 dB as a threshold, below which data were rejected for obtaining reliable Doppler velocity samples at an approximate precision of <0.3 m/s. Vertical velocity variance was then calculated over a 1-min averaging period. According to previous studies (Barlow et al., 2011; Flamant et al., 1997), the gradient in backscatter was used to define the PBL top height, that is, the aerosol-based PBL height, at which the largest gradient between the free atmosphere and PBL occurs. The mixing layer height was defined as the height up to which a threshold of vertical velocity variance above 0.1 m^2/s^2 was met (Barlow et al., 2011).

In addition, based on previous studies (ICAO, 2005; Manninen et al., 2018), wind shear was derived from the available horizontal wind during the velocity azimuth display scans of Doppler lidar as follows:

$$\text{Vector wind shear} = \frac{\left(\Delta u^2 + \Delta v^2\right)^{1/2}}{\Delta z} \quad (1)$$

where Δz is the range gate (30m). u and v are the wind components.

2.2. Meteorological and Air Quality Observations

In addition, hourly PM_{10} and $PM_{2.5}$ (particulate matter, defined as particles with an aerodynamic diameter less than or equal to 10 and 2.5 μm, respectively) data were downloaded from Environmental Protection

Department of Hong Kong (http://www.aqhi.gov.hk/en.html). The observations at two stations [Sha Tin (ST) at 6-m height above sea level (asl) and Tai Po (TP) at 15-m height asl] near the lidar at Physical Geography Experimental Station were averaged to represent the surface air pollution around the lidar station. Data at Tap Mum (TP) at 15-m height asl (a background station) was used to aid the analysis of local and transport air pollutions (see Figure 1). There are many different levels of threshold that may be applied at different locations globally. For example, the Ministry of Ecology and Environment of China/Europe Environment Agency/Environmental Protection Department of Hong Kong categorized exceedance as PM_{10} 24-hr average above 150/50/100 $\mu g/m^3$. We chose the peak values in defining our pollution episodes as 100 $\mu g/m^3$ is more reflective of the more intense pollution events that are of interest in this study, when our lidar observations were available.

According to previous studies (Borge et al., 2007; Guo et al., 2017; Osborne et al., 2019; Zheng et al., 2015), backward trajectories for identified particulate matter pollution episodes were computed using Numerical Atmospheric-dispersion Modelling Environment to identify the impacts of transboundary air pollution and local PM pollution in Hong Kong (Jones et al., 2007). Briefly, the Numerical Atmospheric-dispersion Modelling Environment model is a Lagrangian transport model that is driven by model forecast winds or reanalysis data with variable spatial resolutions (Walters et al., 2017). In this study, meteorological analysis data from the UK's operational global model provide the underlying meteorological driving data, that is, horizontal and vertical components of wind fields at a horizontal resolution of around 10–17 km (10 km post 11 July 2017, and 17 km prior to that) with 70 vertical levels.

Daily weather maps published by the Hong Kong Observation were used to identify the surface synoptic patterns which denote the weather conditions of the episodes. For the peak day of each of the nine identified episodes, the upper air sounding profiles at 08:00 and 20:00 local standard time at King's Park Meteorological Station of Hong Kong Observation were used to validate the lidar observations (Figure 1). This was done by comparing the wind speeds and wind directions from the soundings with those recorded by the lidar at the same time (see Figure S1 in the supporting information). The intercomparison results reveal a good agreement between the Doppler lidar data and the sounding wind profile (Figure S1). The agreement is comparable to the result of Päschke et al. (2015).

3. Results

3.1. Identified Particulate Matter Pollution Episodes

During the study period (excluding our lidar maintenance period), nine elevated PM pollution (EP) episodes (EP1–EP9 in Figure 2) were identified, all of which reveal a daily peak of PM_{10} concentration above 100 $\mu g/m^3$. Our results show that the duration of $PM_{10} > 100$ $\mu g/m^3$ were shorter than 6 hr in all the episodes except in EP7 (~12 hr) and EP9 (~14 hr). The peaks of PM_{10} concentrations at the background site (TM) during most episodes (except for EP2 and EP9) were also >100 $\mu g/m^3$, indicating a minimal spatial variation of PM_{10} during the episodes and thus implying that the episodes were probably related to transport of PM from outside to Hong Kong (Luo et al., 2018). For the weather conditions at the peak time in Table 1, moderate relative humidity (<80%) was observed in most episodes, except for EP5 and EP8, while near-surface wind speed (<3.0 m/s) were rather low in all cases. The near-surface winds in five episodes were less than 1.5 m/s and most included a northerly component. At the time of peak concentrations, surface PM_{10} concentrations during the nine episodes were weakly correlated to wind speed and insignificantly correlated with relative humidity at the surface (Figures 3a and 3b).

In addition, for horizontal pollution features in the PM_{10} peak days, a large-scale higher aerosol optical depth was also usually present around Hong Kong during all nine episodes, based on the combined observations of MODIS onboard Terra and Aqua (see Figure S3). The surface synoptic patterns (see Figure S2 and Table 1) in the PM_{10} peak day were associated with the following classifications: (i) monsoon with a cold high-pressure system over mainland China and with wind convergence (related to EP1, EP5, and EP6, EP9); (ii) saddle-type pressure field (related to EP2), and during cold front passage (related to EP7); (iii) warm high pressure over western North Pacific extending over South China (related to EP3); and (iv) subsidence associated with peripheral circulation of tropical cyclones over northern part of the South China Sea or near Taiwan (related to EP4 and EP8). In general, the surface wind patterns show certain correlations with surface PM concentrations during the episodes, while surface air quality is also closely related to wind

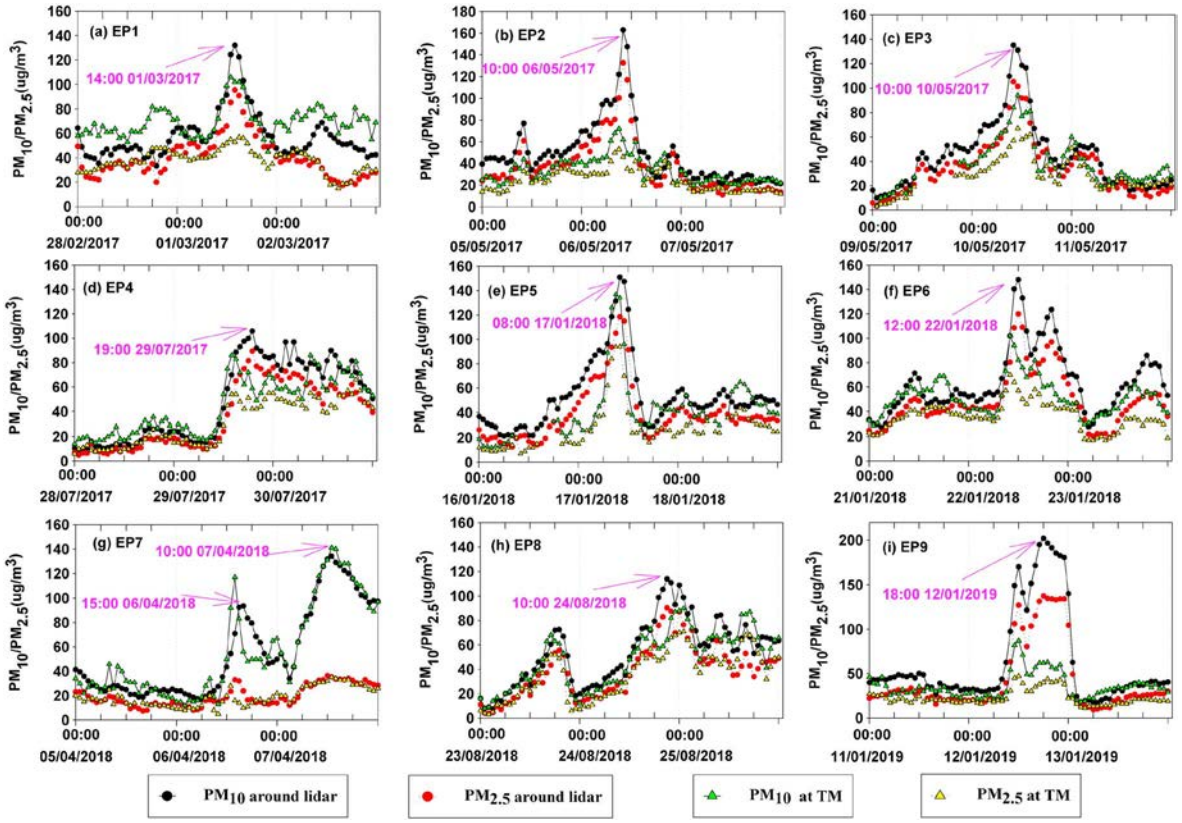

Figure 2. Hourly averaged PM_{10} and $PM_{2.5}$ around lidar station and at Tap Mum (TM) during all particulate matter pollution episodes (EP). The purple arrows indicate the peak time of PM_{10} and $PM_{2.5}$.

at higher altitudes based on the reanalysis data (Tong et al., 2018; Yim et al., 2019), so the vertical wind profiles in the PBL need further exploration.

3.2. Vertical Observations of Particulate Matter Pollution Episodes

Figures 4–6 show time series of lidar data during the nine episodes (over periods of 72 hr): 1-min averages of attenuated backscatter coefficient (log10 scale), 1-min vertical velocity variance, and wind speed every 10 min, indicating that various vertical structures of PBL during these episodes. Compared with time series of surface $PM_{10}/PM_{2.5}$, the backscatter coefficient in PBL usually increased with the increases of surface $PM_{10}/PM_{2.5}$ (Figures 2 and 4). Aerosol backscatter coefficients were higher at the PM_{10} peak time than those at other times during these episodes, excluding the enhanced backscatter by clouds or trace rain based on the meteorological observations at King's Park. Moreover, the high values in near-surface level particulates extended up to approximately 1,000 m at peak time (Figure 4). The backscatter intensities at peak time for EP1, EP2, EP3, EP4, EP6 and EP9 were greater than those for EP5, EP7, EP8, and the vertical thickness of the aerosol backscatter layers varied among episodes, depending on emission sources or weather conditions, i.e. wind speed, turbulent mixing process, and cloud in aerosol-based PBL. For instance, at peak concentration time during the nine episodes, the PM_{10} had a significantly negative correlation [correlation coefficient(r): $r = -0.8652$, $p < 0.01$] with aerosol-based PBL heights derived from vertical backscatter of lidar based on gradient method (Figure 3c). The maximum/minimum peak of PM_{10} are associated with the lowest/highest PBL height of ~1.15/1.75 km for EP9/EP4, suggesting that the role of vertical mixing is important in controlling surface PM concentrations. Here we simply clarify the dependence of PM on aerosol-based PBL height in transport episodes. Note that the correlations also show seasonal variations in both surface PM and aerosol-based PBL height, while there are still some differences in both surface PM and aerosol-based PBL height for different cases in the same season.

Table 1
The Identified PM Pollution Episodes and Their Related Meteorological Conditions During the Periods of February to September 2017 and January 2018 to January 2019

Episodes	Peak day	Peak time (local time)	$PM_{2.5}/PM_{10}$ around lidar station (at TM) ($\mu g/m^3$)	RH (%)	WD (°)	WS (m/s)	Synoptic pattern at surface (refer to Figure S2 in the supporting information)
EP1	1/3/20-17	14:00	96/132 (53/106)	54	340	1.3	Monsoon associated with cold high pressure, local surface wind convergence
EP2	6/5/20-17	10:00	133/163 (46/62)	68	300	0.7	Saddle type pressure field, weak surface wind convergence
EP3	10/5/20-17	10:00	105/135 (57/84)	74	280	0.5	Warm high pressure over the western North Pacific extending over South China
EP4	29/7/20-17	19:00	90/106 (42/59)	77	290	2.1	Subsidence associated with the peripheral circulation of tropical cyclones over the South China Sea and near Taiwan
EP5	17/1/20-18	08:00	119/151 (97/137)	82	270	0.1	Monsoon associated with cold high pressure, weak surface wind convergence
EP6	22/1/20-18	12:00	120/148 (57/82)	70	290	0.4	Monsoon associated with cold high pressure
EP7	07/4/20-18	10:00	36/136 (35/141)	43	50	2.9	Cold front passage, northerly wind related to dust storm
EP8	24/8/20-18	19:00	91/114 (47/57)	80	250	2.1	Subsidence associated with the peripheral circulation of a tropical cyclone near Taiwan, local surface wind convergence
EP9	12/1/20-19	18:00	139/202 (40/62)	76	260	1.2	Monsoon associated with cold high pressure, local surface wind convergence

RH: relative humidity; WD: wind direction; WS: wind speed.

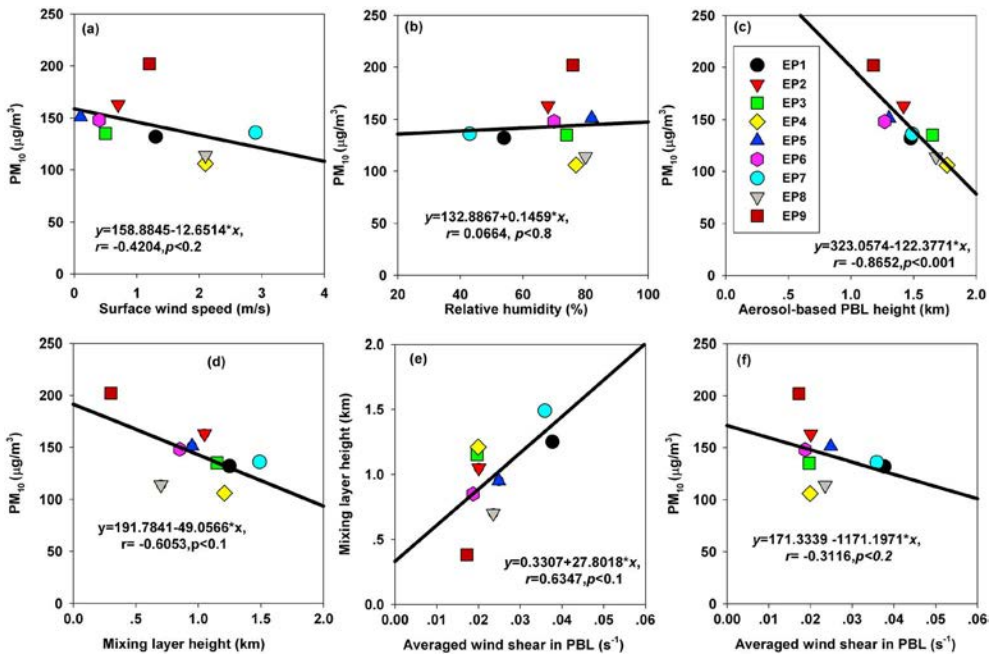

Figure 3. Scatterplot and linear regressions of surface PM_{10} and (a) surface wind speed, (b) relative humidity, (c) aerosol-based PBL heights, (d) mixing layer heights, and linear regressions of averaged wind shear in PBL and (e) mixing layer heights, and (f) surface PM_{10} at peak time.

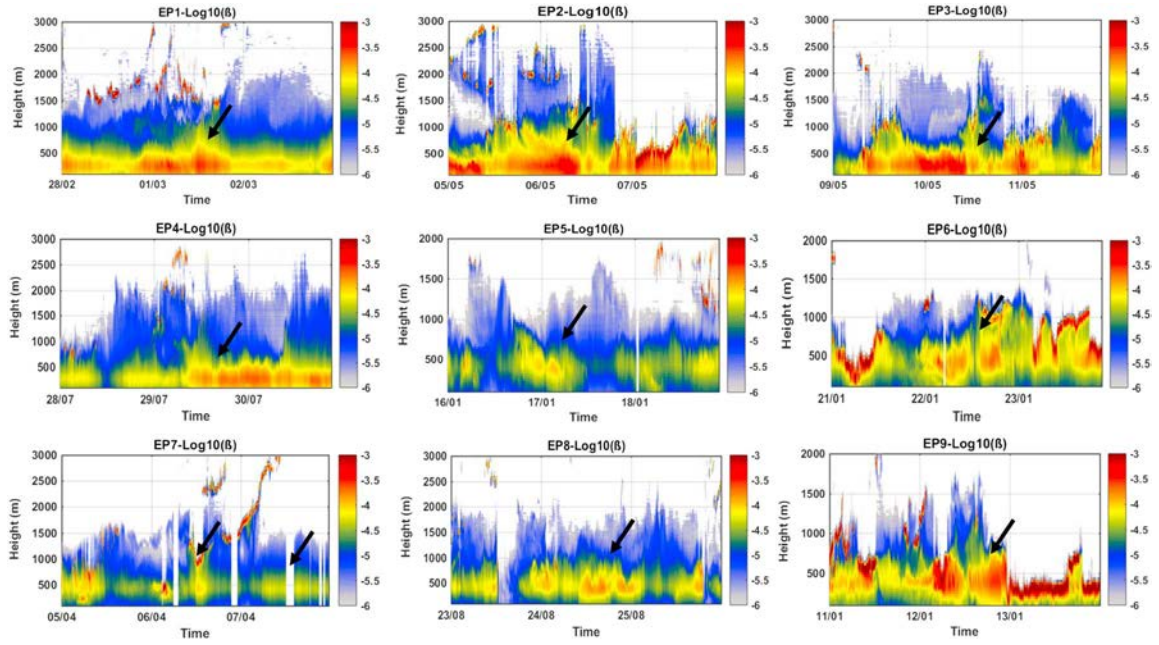

Figure 4. Diurnal variations in 1-min average of aerosol backscatter values β (m/sr; log10 scale) during nine episodes, and the black arrows indicate the peak time of PM_{10}.

It should be noted that the smaller the vertical velocity variance is, the more stable the atmosphere is. Stable atmospheric conditions are conducive to the accumulation of air pollutants in the PBL. From the time series of vertical velocity variance and wind speed, it can be clearly seen that different turbulent mixing intensities appeared during the nine episodes. At the time of peak concentrations, stronger turbulence with larger vertical velocity variances (>0.1 m^2/s^2) were evident in the whole PBLs in EP1, EP4, and EP7 (Figure 5), showing that higher mixing layer heights (Figure 3d) were probably related to strong transport under strong wind speed conditions (>7 m/s in the whole PBL; Figure 6). In EP2, EP5, EP6, and EP8, strong turbulence with larger vertical velocity variances (>0.1 m^2/s^2) only occurred at near surface (<500 m asl) with strong wind speeds at upper PBL before peak time (Figure 6). Very weak turbulence with smaller vertical velocity variances (<0.1 m^2/s^2) mainly appeared in the whole PBLs in EP3 and EP9 (Figure 3d), indicating that a stable condition with low mixing layer heights is conducive to local pollutant accumulations under very weak wind speed (<2 m/s in the whole PBL; Figure 6). The correlation between mixing layer heights and the surface PM_{10} at peak time during the nine episodes also show a strong inversion correlation ($r = -0.8316$, $p < 0.01$). The maximum/minimum peak of PM_{10} are associated with the lowest/highest mixing layer height of ~0.3/1.5 km for EP9/EP4. In general, before or at the peak of most episodes (EP1, EP2 EP4, EP5, EP6, EP7, and EP8), wind speed increased, and meanwhile, the wind direction changed to north (Figure S4) in the whole or upper PBLs, indicating that PM transboundary episodes in Hong Kong are usually accompanied with a relatively large wind speed from upstream high-emission regions of mainland China.

According to previous study (Osborne et al., 2019), we employed the Numerical Atmospheric-dispersion Modelling Environment backward trajectory analysis described in section 2 to explore the source of air mass that transported PM to Hong Kong. Figure 7 shows the horizontal and vertical components of 72-hr backward trajectory of our lidar in Physical Geography Experimental Station at The Chinese University of Hong Kong during the nine episodes. Based on the vertical aerosol backscatter, the starting trajectory heights were from 100 to 1,000 m with an interval of 100 m, and the initial times were set to the peak time of PM_{10} of each episode. Generally, all the air masses of Hong Kong during these episodes originated from mainland China. From the vertical component, there were obvious descending trends during the past 72 hr of these episodes, and the results show that the transboundary air pollution altitudes in the PBL varied among episodes.

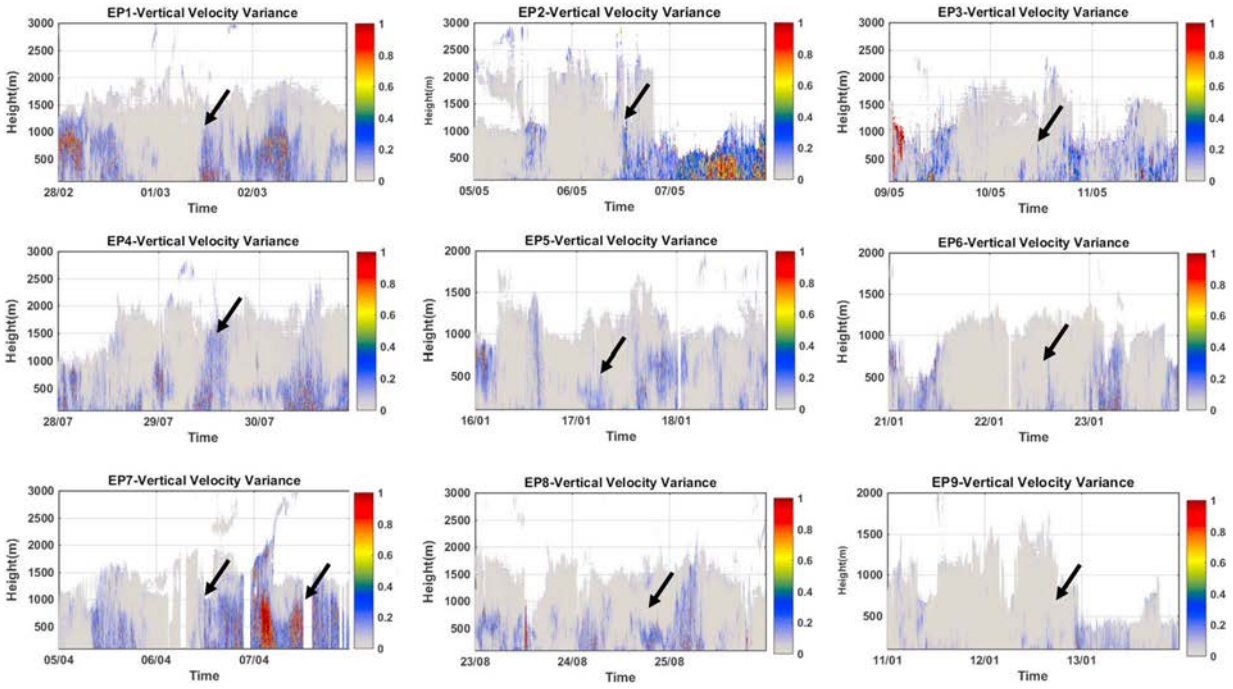

Figure 5. Same as Figure 4 but for vertical velocity variances.

With respect to relative contributions among the different emission source regions, Hou et al. (2018) defined two classifications of transboundary air pollution in the PRD regions as follows: regional transboundary air pollution (between cities in the PRD region) and superregional transboundary air pollution (from outside of the PRD region). In this study, superregional (regional) transboundary air pollution was identified when air mass in Hong Kong in one episode came from outside (within) the PRD region within 72 hr based on the backward trajectories. Notably, our use of backward trajectories was to identify possible sources of the heavy air pollution episodes in Hong Kong. We would like to clarify that our episode naming convention was designed to highlight particular features of the episodes. For example, regional transbounary EP means regional sources had remarkably contributed to the episode, whereas local contribution is not necessary to be insignificant. The name was chosen to highlight the regional transboundary air pollution feature in the episode. It should also be noted that a trajectory from superregion to Hong Kong must pass through the PRD region. As mentioned above, when the 72-hr backward trajectory indicated a superregional contribution, the regional and local contributions could be also important. Generally, it can be clearly seen from Figure 7 that EP3, EP5, EP6, and EP9 were related to regional transboundary air pollution for Hong Kong, while the others (EP1, EP2, EP4, EP7, and EP8) were associated with superregional transboundary air pollution. Particularly, EP4 was a very long distance transboundary air pollution event related to a dust storm event in northern China, in which the strong wind brought the dust belt of high PM_{10} concentrations with a large ratio of PM_{10} and $PM_{2.5}$ from northern China to southern China during 03–07 April 2018 (Figures S5 and S6). As a result, when the dust storm and accompanying strong northerly winds in the whole PBL (Figures 6 and S3) reached Hong Kong on 6 and 7 April, the surface PM_{10} increased abruptly and exhibited peaks, while $PM_{2.5}$ had no peak in our observations (Figure 2).

3.3. Relationships Between Surface Particulate Matters and Vertical Wind Profiles

To assess the observed transboundary air pollution path and height related to wind profiles in Hong Kong, Figure 8 shows the correlation coefficients between hourly wind speed in each layer and hourly surface PM_{10} during 72/48/24 hr (peak day) for nine episodes, and 1-hr-lag hourly surface PM_{10} during 24 hr (peak day), indicating the various relationships between surface particulate matter and vertical wind profiles.

In detail, the relationships were significantly positive at different PBL heights in most episodes (EP1, EP4, EP5, EP7, EP8, and EP9), suggesting that the higher the wind speed was, the heavier the pollution was. It

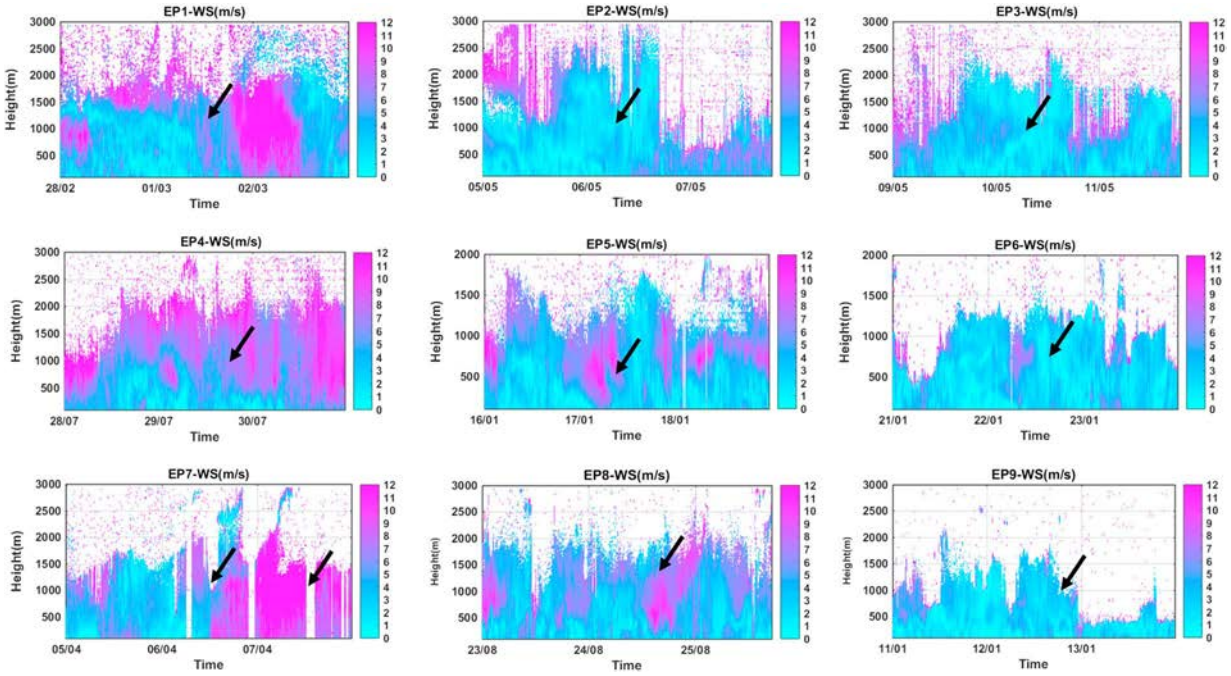

Figure 6. Same as Figure 4 but for wind speed.

indicates that the wind speeds in these PBL heights show positive contributions to the pollutant concentration on the ground, which were different from the negative statistical relationships between surface wind speed and surface PM at peak time for these nine episodes (Figure 3a). Our results show that the large wind speed caused pollutants from mainland China to be transported to Hong Kong before or at peak time, which can be clearly observed by higher MODIS-based aerosol optical depth or higher ground-based PM concentrations in the upstream mainland China regions (see Figures S3, S5, and S6). In addition, the significant-correlation heights in Figure 8 ranging from 200 to 2,000 m can be considered as the transport path and layer of regional or superregional pollutants during these episodes. In contrast, the relationships between hourly wind speed and hourly surface PM_{10} were significantly negative at most heights of the PBL in EP2, EP3, and EP6, suggesting that the lower the wind speed was, the heavier the surface PM pollution was, because the wind speed in the whole PBL were relatively weak (Figure 6). This is similar to the negative statistical relationships between surface wind speed and surface PM at peak time in these nine episodes (Figure 3a).

Wind shear is a source of turbulent mixing. At peak time in the nine episodes, the averaged wind shears in PBL were positively related to mixing layer heights and negatively related to surface PM_{10} (Figures 2e and 2f), respectively, implying that the larger the averaged wind shear was, the stronger turbulent mixing was and thus the lower surface PM level was. However, the variability in the correlation coefficients between hourly vertical wind shear and hourly surface PM_{10} shows that turbulence mixing process at different heights in the PBL influenced surface PM_{10} (Figure 9). Compared with vertical wind speed and vertical velocity variance (Figures 5 and 6), in EP2, EP3, EP6, and EP9, wind speeds in the whole PBL were relatively weak, and the wind shear and mixing process were small. The relationship between hourly vertical wind shear and hourly surface PM_{10} mainly shows negative correlations at certain heights in the PBL. In EP1, EP4, EP5, EP7, and EP8, wind speeds in the whole PBL were relatively strong, and the wind shear and mixing process were strong. The relationship between hourly vertical wind shear and hourly surface PM_{10} generally exhibited positive correlations at certain heights in the PBL, especially near surface. The high transboundary PM was due to the upper level strong wind transporting PM to Hong Kong, and the PM then impacted surface PM concentrations at the ground through the vertical turbulent exchange in the PBL (Figure 5) to abruptly cause a significant increase in surface PM, which can be demonstrated by that the thicker layer of high-backscatter usually appeared around peak time due to the mixing of local PM and transboundary PM (Figure 4).

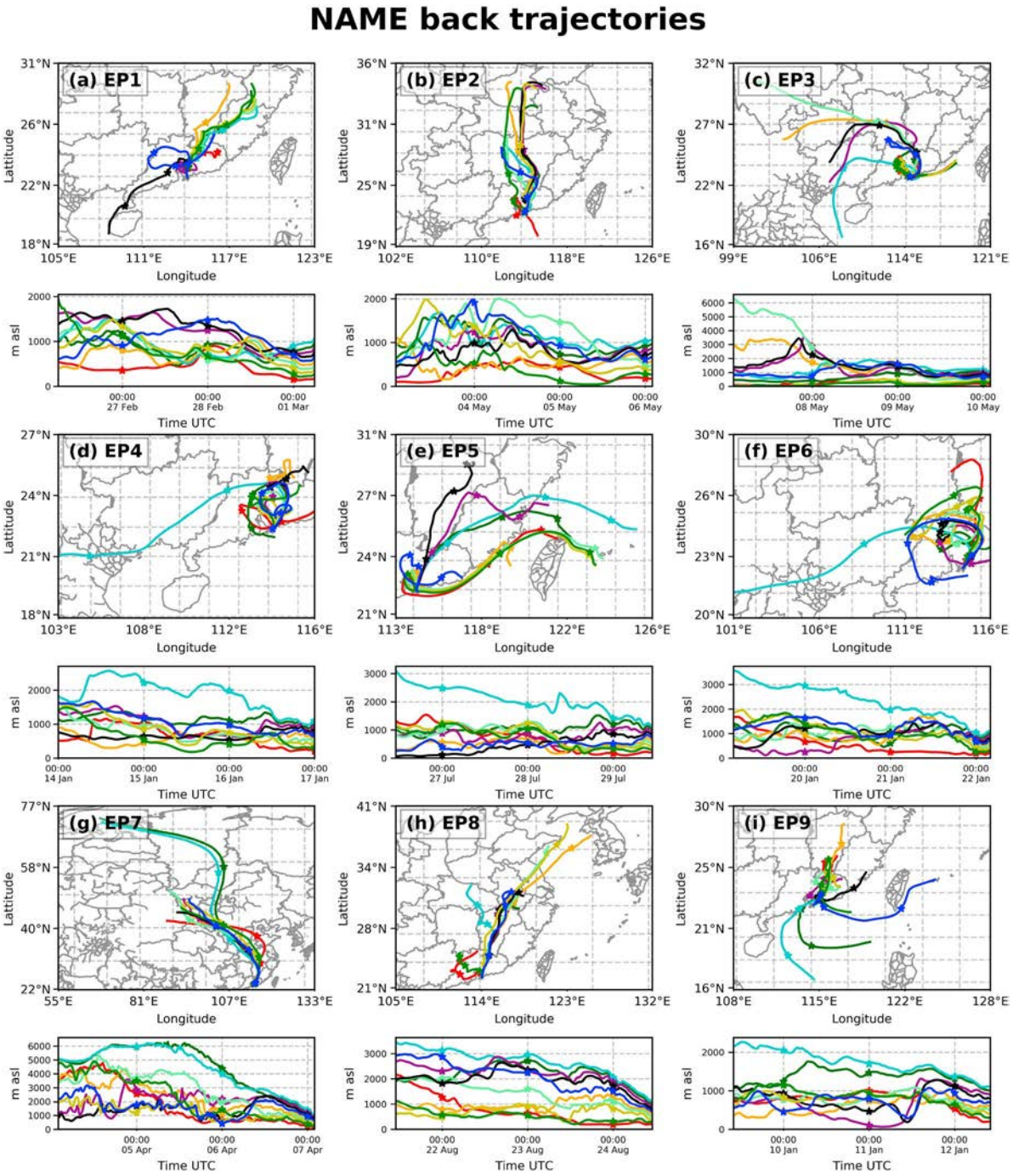

Figure 7. The horizontal and vertical components of 72-hr backward trajectory of lidar station in PGES at CUHK during these nine episodes: (a) EP1, (b) EP2, (c) EP3, (d) EP4, (e) EP5, (f) EP6, (g) EP7, (h) EP8, and (i) EP9.

4. Discussion

Transboundary PM pollution is one of the important contributors to air pollution episodes in Hong Kong as shown in various previous typical cases and long-term statistical studies (Chung et al., 1999; Hou et al., 2018; Lam et al., 2018; Liu & Chan, 2002; Louie et al., 2005; Luo et al., 2018; Tong et al., 2018; Yim et al., 2019). The previous studies particularly pointed out that northerly winds are favorable for long-range transport from

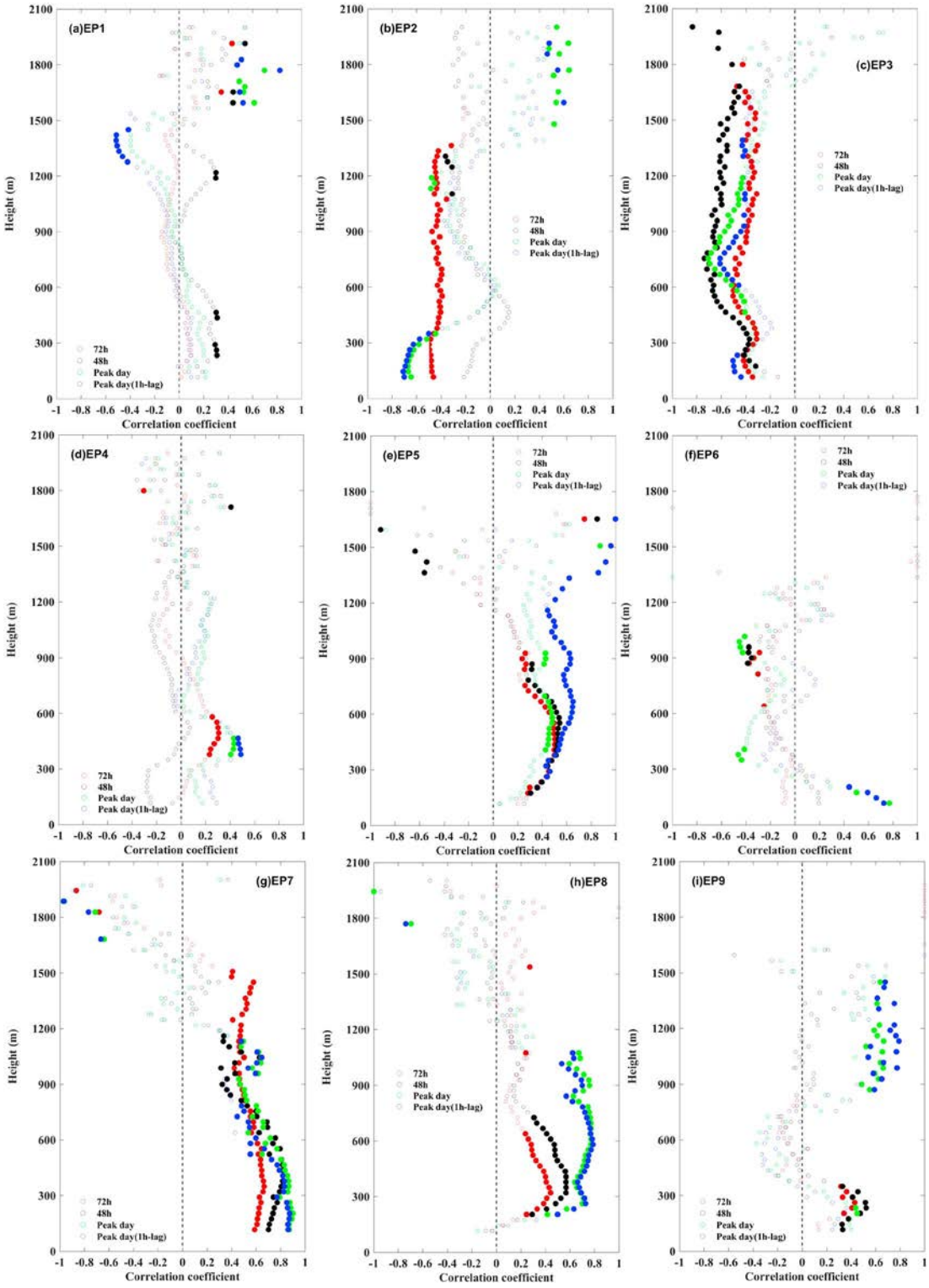

Figure 8. The correlation coefficients between hourly wind speed in each layer and hourly surface PM_{10}/1-hr-lag hourly surface PM_{10} during 72 hr (red), 48 hr (black), and 24 hr of peak day (green/blue) for nine episodes. The filled circles indicate correlation significance passed the 95% confidence level.

mainland China leading to pollutant accumulation in a stable atmosphere. They also found that northerly winds are usually associated with the four typical kinds of weather conditions that this study summarized, including surface high pressure, cold front, dust storm, and typhoon regimes.

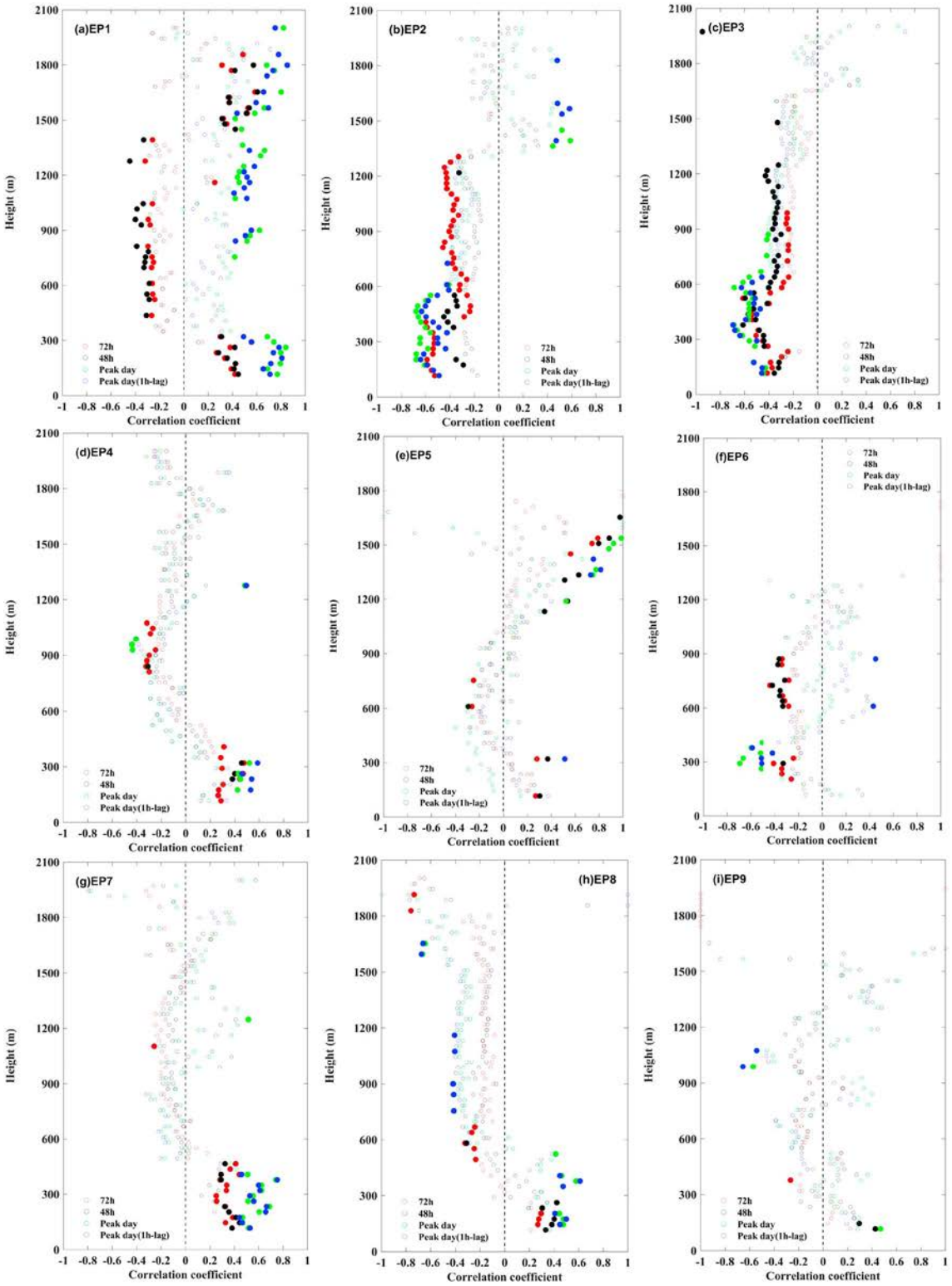

Figure 9. Same for Figure 8 but for wind shear and PM_{10}.

Moreover, based on surface observations with vertical reanalysis data and back trajectory models, the previous studies indicated that meteorological variables at various altitudes (to ~700 hPa) played an important role in influencing surface air quality (Tong et al., 2018). For instance, the strengthened and higher frequency of northerly wind at higher levels in atmosphere (>900 hPa) could increase the transboundary air pollution contribution to Hong Kong, especially in winter or under the influence of a tropical cyclone (Luo et al., 2018; Yim et al., 2019). With the available vertical high-resolution observations, our study shows that the studied nine episodes exhibited vertical differences in the lidar backscatter profile and correlation with vertical wind speeds. This implies that there were different transport pathways and heights, and the maximum transport height extended from surface to about 2.0 km or even higher in superregional or regional transboundary EPs related to nonlocal emission contributions.

For relative nonlocal emission contributions, Luo et al. (2018) applied an integrated statistical scheme to estimate the contributions of transboundary air pollution to PM pollutants over Hong Kong. The authors reported that the relative contribution of nonlocal sources to annual PM can reach 80%. Hou et al. (2018) further applied state-of-the-art atmospheric modeling to estimate that approximately 60% and 20% of annual PM were respectively attributable to superregional contributions (emissions outside the PRD region) and regional contributions (emissions inside the PRD region). For instance in our present work, EP4 and EP8 were the EPs related to typhoons as superregional contributions, with PM_{10} concentrations breaching safe air quality thresholds (Figures 2, 4, and 7). According to previous studies (Lam et al., 2018; Luo et al., 2018), transboundary air pollution related to typhoons possibly increases transported PM_{10} from mainland China to Hong Kong by 46–70%. Therefore, the superregional contribution is one important contributor to ambient PM in Hong Kong. The cause of the difference between superregional and regional contributions can be explained by our high-resolution vertical observations (Figures 4 and 8) as follows: compared to most regional transboundary EPs (except for EP5), the aerosol layers were more elevated above 1 km, while PM were also more positively correlated with high-level or even whole-PBL wind speeds in most superregional transboundary EPs (EP1, EP2, EP4, EP7, and EP8), which may be favorable for more transported pollutions.

In general, our intention is to document the utility of the lidar system in diagnosing large-scale transboundary air pollution over Hong Kong. We are currently developing a lidar system network to collect more samples of events in the PRD region; it should then be possible to generalize the results by clustering the analyses in the whole PRD region. Nevertheless, our identified EPs provided useful cases for detailed investigations through modeling and statistical methods. This study is expected to assist future modeling studies for improving the model capability to accurately simulate vertical distribution of air pollution. It should also be noted that the Doppler lidar provides a powerful measurement tool for real-time monitoring, forecast, and assessment of air pollution.

5. Conclusion

In this study, we employed high-time-resolution vertical observations from Doppler lidar to explore heavy particulate matter pollution episodes in Hong Kong. Nine EPs were identified and analyzed, of which transboundary EPs were associated with surface cold/warm high-pressure system, surface pressure field of the saddle type, cold front passes, or peripheral circulation of typhoons to the northeast of Hong Kong. The relationships between vertical aerosol backscatter with surface particulate matter and vertical wind profiles during these nine EPs were investigated in detail. The conclusions are summarized as follows.

For aerosol backscatter coefficient, the values were higher in the PM_{10} peak time than those at other times during these episodes; meanwhile, the thicker layer of high backscatter usually appeared around peak particulate matter time due to the mixing of local PM and transboundary PM. In most episodes, before or at peak time, wind speed increased and the wind direction changed to the north in the whole or upper PBLs, indicating that PM transboundary episodes in Hong Kong were influenced by the high upstream emissions of mainland China. These EPs were closely related to various vertical wind profiles in the PBL, which suggest that strong vertical wind speed with wind shear at certain heights of PBL had a positive correlation with surface PM during most superregional transboundary EPs. The averaged wind shear in PBL were positively related to mixing layer heights and negatively related to surface PM_{10} at peak time, respectively.

These EPs with different mixing layer heights were mainly driven by different vertical wind shear under various weather systems related to surface high pressure, cold front, dust storm, and typhoon. The maximum transport height extended from the surface to about 2.0 km or even higher, which were different among superregional and regional transboundary EPs. In general, our findings provide scientific evidence that surface PM pollutions were closely related to the characteristics of vertical profiles during transboundary air pollutions observed by high-time-resolution Doppler lidar.

Acknowledgments
This work was jointly funded by The Vice-Chancellor's Discretionary Fund of The Chinese University of Hong Kong (grant 4930744), the Early Career Scheme of Research Grants Council of Hong Kong (grant ECS-24301415), and the Chinese University of Hong Kong - University of Exeter Joint Centre for Environmental Sustainability and Resilience (ENSURE) (CUHK Project No.: 4930810). We would like to thank the Hong Kong Environmental Protection Department, the Hong Kong Observatory, Ministry of Ecology and Environment of China, and NASA for providing the air quality data, meteorological data, particulate matter data, and aerosol optical depth data, respectively. PM_{10} and $PM_{2.5}$ data were downloaded from Environmental Protection Department of Hong Kong (http://www.aqhi.gov.hk/en.html) and Data Center of Ministry of Ecology and Environment of China (http://106.37.208.233:20035/). Backward trajectories with meteorological analysis data were supplied by the UK Meteorological Office (https://www.metoffice.gov.uk/research/modelling-systems/dispersion-model). The Hong Kong meteorological data were obtained from the Hong Kong Observation (https://www.hko.gov.hk/cis/climat_e.htm). The merged MODIS-based aerosol optical depth (AOD) was obtained from NASA's Earth Observing System Data and Information System (https://worldview.earthdata.nasa.gov/). The authors declare no competing financial interest.

References

Barlow, J. F., Dunbar, T. M., Nemitz, E. G., Wood, C. R., Gallagher, M. W., Davies, F., et al. (2011). Boundary-layer dynamics over London, UK, as observed using Doppler lidar during REPARTEE-II. *Atmospheric Chemistry and Physics*, *11*(5), 2111–2125. https://doi.org/10.5194/acp-11-2111-2011

Borge, R., Lumbreras, J., Vardoulakis, S., Kassomenos, P., & Rodríguez, E. (2007). Analysis of long-range transport influences on urban PM_{10} using two-stage atmospheric trajectory clusters. *Atmospheric Environment*, *41*(21), 4434–4450. https://doi.org/10.1016/j.atmosenv.2007.01.053

Cai, W., Li, K., Liao, H., Wang, H., & Wu, L. (2017). Weather conditions conducive to Beijing severe haze more frequent under climate change. *Nature Climate Change*, *7*(4), 257–262. https://doi.org/10.1038/NCLIMATE3249

Chung, K. K., Chan, J. C. L., Ng, C. N., Lam, K. S., & Wang, T. (1999). Synoptic conditions associated with high carbon monoxide episodes at a coastal station in Hong Kong. *Atmospheric Environment*, *33*(19), 3087–3095. https://doi.org/10.1016/S1352-2310(97)00328-2

Fan, Q., Shen, C., Wang, X. M., Li, Y., Huang, W., Liang, G. X., et al. (2013). Impact of a dust storm on characteristics of particle matter (PM) in Guangzhou, China. *Asia-Pacific Journal of Atmospheric Sciences*, *49*(4), 121–131.

Fan, W., Qin, K., Xu, J., Yuan, L., Li, D., Jin, Z., & Zhang, K. (2019). Aerosol vertical distribution and sources estimation at a site of the Yangtze River Delta region of China. *Atmospheric Research*, *217*, 128–136. https://doi.org/10.1016/j.atmosres.2018.11.002

Flamant, C., Pelon, J., Flamant, P. H., & Durand, P. (1997). Lidar determination of the entrainment zone thickness at the top of the unstable marine atmospheric boundary layer. *Boundary-Layer Meteorology*, *83*(2), 247–284. https://doi.org/10.1023/A:1000258318944

Gu, Y., Wai, W. T., Law Stephen, C. K., Hui, D. G., Ho, K. F., Yuanjian, Y., & Lam, Y. S. H. (2018). Impacts of sectoral emissions in China and the implications: Air quality, public health, crop production, and economic costs. *Environmental Research Letters*, *13*(8). https://doi.org/10.1088/1748-9326/aad138

Gu, Y., & Yim, S. H. L. (2016). The air quality and health impacts of domestic trans-boundary pollution in various regions of China. *Environment International*, *97*, 117–124. https://doi.org/10.1016/j.envint.2016.08.004

Guo, J. P., He, J., Liu, H. L., Miao, Y. C., Liu, H., & Zhai, P. M. (2016). Impact of various emission control schemes on air quality using WRF-Chem during APEC China 2014. *Atmospheric Environment*, *140*, 311–319. https://doi.org/10.1016/j.atmosenv.2016.05.046

Guo, J. P., Lou, M. Y., Miao, Y. C., Wang, Y., Zeng, Z. L., Liu, H., et al. (2017). Trans-Pacific transport of dust aerosol originated from East Asia: Insights gained from multiple observations and modeling. *Environmental Pollution*, *230*, 1030–1039. https://doi.org/10.1016/j.envpol.2017.07.062

Guo, J. P., Zhang, X. Y., Wu, Y. R., Zhaxi, Y. Z., Che, H. Z., La, B., et al. (2011). Spatio-temporal variation trends of satellite-based aerosol optical depth in China during 1980–2008. *Atmospheric Environment*, *45*(37), 6802–6811. https://doi.org/10.1016/j.atmosenv.2011.03.068

Harvey, N. J., Hogan, R. J., & Dacre, H. F. (2013). A method to diagnose boundary-layer type using Doppler lidar: A method to diagnose boundary-layer type. *Quarterly Journal of the Royal Meteorological Society*, *139*(676), 1681–1693. https://doi.org/10.1002/qj.2068

He, Q., Li, C., Mao, J., Lau, K. H., & Chu, D. A. (2008). Analysis of aerosol vertical distribution and variability in Hong Kong. *Journal of Geophysical Research*, *113*, D14211. https://doi.org/10.1029/2008JD009778

Hou, X., Chan, C. K., Dong, G. H., & Yim, S. H. (2018). Impacts of transboundary air pollution and local emissions on PM2.5 pollution in the Pearl River Delta region of China and the public health, and the policy implications. *Environmental Research Letters*, *14*(3). https://doi.org/10.1088/1748-9326/aaf493

ICAO (2005). Manual on low-level wind shear (Tech. rep.): International Civil Aviation Organization.

Jones, A., Thomson, D., Hort, M., & Devenish, B. (2007). The UK Met Office's next-generation atmospheric dispersion model, NAME III. In *Air pollution modeling and its application XVII*, (pp. 580–589). Boston, MA: Springer.

Kang, H., Zhu, B., Gao, J., He, Y., Wang, H., Su, J., et al. (2019). Potential impacts of cold frontal passage on air quality over the Yangtze River Delta, China. *Atmospheric Chemistry and Physics*, *19*(6), 3673–3685. https://doi.org/10.5194/acp-19-3673-2019

Lam, Y. F., Cheung, H. M., & Ying, C. C. (2018). Impact of tropical cyclone track change on regional air quality. *Science of the Total Environment*, *610-611*, 1347–1355. https://doi.org/10.1016/j.scitotenv.2017.08.100

Li, Z., Guo, J., Ding, A., Liao, H., Liu, J., Sun, Y., et al. (2017). Aerosol and boundary-layer interactions and impact on air quality. *National Science Review*, *4*(6), 810–833. https://doi.org/10.1093/nsr/nwx117

Li, Z., Lau, W. K. M., Ramanathan, V., Wu, G., Ding, Y., Manoj, M. G., et al. (2016). Aerosol and monsoon climate interactions over Asia. *Reviews of Geophysics*, *54*, 866–929. https://doi.org/10.1002/2015RG000500

Liang, P. F., Zhu, T., Fang, Y. H., Li, Y. G., Han, Y. Q., Wu, Y. S., et al. (2017). The role of meteorological conditions and pollution control strategies in reducing air pollution in Beijing during APEC 2014 and Victory Parade 2015. *Atmospheric Chemistry and Physics*, *17*(22), 13,921–13,940. https://doi.org/10.5194/acp-17-13921-2017

Liu, D., Yang, Y., Cheng, Z., Huang, H., Zhang, B., Ling, T., & Shen, Y. (2013). Retrieval and analysis of a polarized high-spectral-resolution lidar for profiling aerosol optical properties. *Optics Express*, *21*(11), 13,084–13,093. https://doi.org/10.1364/OE.21.013084

Liu, F., Zhang, Q., Tong, D., Zheng, B., Li, M., Huo, H., & He, K. B. (2015). High-resolution inventory of technologies, activities, and emissions of coal-fired power plants in China from 1990 to 2010. *Atmospheric Chemistry and Physics*, *15*(13), 18,787–18,837.

Liu, H., & Chan, J. C. L. (2002). An investigation of air-pollutant patterns under sea–land breezes during a severe air-pollution episode in Hong Kong. *Atmospheric Environment*, *36*(4), 591–601. https://doi.org/10.1016/S1352-2310(01)00504-0

Louie, P. K., Watson, J. G., Chow, J. C., Chen, A., Sin, D. W., & Lau, A. K. (2005). 5Seasonal characteristics and regional transport of $PM_{2.5}$ in Hong Kong. *Atmospheric Environment*, *39*(9). https://doi.org/10.1016/j.atmosenv.2004.11.017

Luo, M., Hou, X., Gu, Y., Lau, N. C., & Yim, S. H. L. (2018). Trans-boundary air pollution in a city under various atmospheric conditions. *Science of the Total Environment*, *618*, 132–141. https://doi.org/10.1016/j.scitotenv.2017.11.001

Manninen, A. J., Marke, T., Tuononen, M., & O'Connor, E. J. (2018). Atmospheric boundary layer classification with Doppler lidar. *Journal of Geophysical Research: Atmospheres*, *123*, 8172–8189. https://doi.org/10.1029/2017JD028169

Miao, Y., Guo, J., Liu, S., Liu, H., Li, Z., Zhang, W., & Zhai, P. (2017). Classification of summertime synoptic patterns in Beijing and their associations with boundary layer structure affecting aerosol pollution. *Atmospheric Chemistry and Physics*, *17*, 1–33.

Miao, Y. C., Hu, X. M., Liu, S. H., Qian, T. T., Xue, M., Zheng, Y. J., & Wang, S. (2015). Seasonal variation of local atmospheric circulations and boundary layer structure in the Beijing-Tianjin-Hebei region and implications for air quality. *Journal of Advances in Modeling Earth Systems*, *7*, 1–25. https://doi.org/10.1002/2015MS000522

Mok, T. M., & Rudowicz, C. Z. (2004). A lidar study of the atmospheric entrainment zone and mixed layer over Hong Kong. *Atmospheric Research*, *69*(3–4), 147–163. https://doi.org/10.1016/j.atmosres.2003.09.004

Orru, H., Ebi, K. L., & Forsberg, B. (2017). The interplay of climate change and air pollution on health. *Current Environmental Health Reports*, *4*(4), 504–513. https://doi.org/10.1007/s40572-017-0168-6

Osborne, M., Malavelle, F. F., Adam, M., Buxmann, J., Sugier, J., Marenco, F., & Haywood, J. (2019). Saharan dust and biomass burning aerosols during ex-hurricane Ophelia: Observations from the new UK lidar and Sun-photometer network. *Atmospheric Chemistry and Physics*, *19*(6), 3557–3578. https://doi.org/10.5194/acp-19-3557-2019

Päschke, E., Leinweber, R., & Lehmann, V. (2015). An assessment of the performance of a 1.5 μm Doppler lidar for operational vertical wind profiling based on a 1-year trial. *Atmospheric Measurement Techniques*, *8*(6), 2251–2266. https://doi.org/10.5194/amt-8-2251-2015

Pearson, G., Davies, F., & Collier, C. (2010). Remote sensing of the tropical rain forest boundary layer using pulsed Doppler lidar. *Atmospheric Chemistry and Physics*, *10*(13), 5891–5901. https://doi.org/10.5194/acp-10-5891-2010

Qi, Y., Li, W., & Zhang, H. (2014). Local and inter-regional contributions to $PM_{2.5}$ nitrate and sulfate in China. *Atmospheric Environment*, *94*, 582–592.

Qin, K., Wu, L., Wong, M. S., Letu, H., Hu, M., Lang, H., et al. (2016). Trans-boundary aerosol transport during a winter haze episode in China revealed by ground-based lidar and CALIPSO satellite. *Atmospheric Environment*, *141*, 20–29. https://doi.org/10.1016/j.atmosenv.2016.06.042

Su, T., Li, J., Li, C., Xiang, P., Lau, A. K. H., Guo, J., et al. (2017). An intercomparison of long-term planetary boundary layer heights retrieved from CALIPSO, ground-based lidar, and radiosonde measurements over Hong Kong. *Journal of Geophysical Research: Atmospheres*, *122*, 3929–3943. https://doi.org/10.1002/2016JD025937

Su, T. N., Li, Z. Q., & Kahn, R. (2018). Relationships between the planetary boundary layer height and surface pollutants derived from lidar observations over China: Regional pattern and influencing factors. *Atmospheric Chemistry and Physics*, *18*(21), 15,921–15,935. https://doi.org/10.5194/acp-18-15921-2018

Tong, C. H. M., Yim, S. H. L., Rothenberg, D., Wang, C., Lin, C. Y., Chen, Y., & Lau, N. C. (2018). Assessing the impacts of seasonal and vertical atmospheric conditions on air quality over the Pearl River Delta region. *Atmospheric Environment*, *180*, 69–78. https://doi.org/10.1016/j.atmosenv.2018.02.039

Walters, D., Boutle, I., Brooks, M., Melvin, T., Stratton, R., Vosper, S., et al. (2017). The Met Office unified model global atmosphere 6.0/6.1 and JULES global land 6.0/6.1 configurations. *Geoscientific Model Development*, *10*(4), 1487–1520. https://doi.org/10.5194/gmd-10-1487-2017

Wang, T., Fei, J., Deng, J., Shen, Y., Fu, Q., Wang, Q., et al. (2012). Urban air quality and regional haze weather forecast in Yangtze River Delta of China. *Atmospheric Environment*, *58*, 70–83. https://doi.org/10.1016/j.atmosenv.2012.01.014

Xing, C., Liu, C., Wang, S., Chan, K. L., Gao, Y., Huang, X., et al. (2017). Observations of the vertical distributions of summertime atmospheric pollutants and the corresponding ozone production in Shanghai, China. *Atmospheric Chemistry and Physics*, *17*, 14,275–14,289. https://doi.org/10.5194/acp-17-14275-2017

Yang, D., Li, C., Lau, A. K. H., & Li, Y. (2013). Long-term measurement of daytime atmospheric mixing layer height over Hong Kong. *Journal of Geophysical Research: Atmospheres*, *118*, 2422–2433. https://doi.org/10.1002/jgrd.50251

Yang, Y., Zheng, X., Gao, Z., Wang, H., Wang, T., Li, Y., et al. (2018). Long-term trends of persistent synoptic circulation events in planetary boundary layer and their relationships with haze pollution in winter half-year over eastern China. *Journal of Geophysical Research: Atmospheres*, *123*, 10,991–11,007. https://doi.org/10.1029/2018JD028982

Yim, S. H. L., & Barrett, S. R. H. (2012). Public health impacts of combustion emissions in the United Kingdom. *Environmental Science & Technology*, *46*(8), 4291–4296. https://doi.org/, https://doi.org/10.1021/es2040416

Yim, S. H. L., Gu, Y., Shapiro, A. M., & Stephens, B. (2019) Air quality and acid deposition impacts of local emissions and transboundary air pollution in Japan and South Korea. Accepted to be published in *Atmospheric Chemistry and Physics*. https://doi.org/10.5194/acp-2019-175

Yim, S.H.L., Hou, X., Guo, J., & Yang, Y. (2019). Contribution of local emissions and transboundary air pollution to air quality in Hong Kong during El Niño-Southern Oscillation and heatwaves. *Atmospheric Research*, *218*, 50–58.

Zhang, Z., Wenig, M., Zhou, W., Diehl, T., Chan, K. L., & Wang, L. (2014). The contribution of different aerosol sources to the aerosol optical depth in Hong Kong. *Atmospheric Environment*, *83*, 145–154. https://doi.org/10.1016/j.atmosenv.2013.10.047

Zheng, X.-Y., Fu, Y.-F., Yang, Y.-J., & Liu, G.-S. (2015). Impacts of atmospheric circulations on aerosol distributions in autumn over eastern China: Observational evidences. *Atmospheric Chemistry and Physics*, *15*, 12,115–12,138. https://doi.org/10.5194/acp-15-12115-201

Zheng, Z., Li, Y., Wang, H., Ding, H., Li, Y., Gao, Z., & Yang, Y. (2019). Re-evaluating the variation in trend of haze days in the urban areas of Beijing during a recent 36-year period. *Atmospheric Science Letters*, *20*(1). https://doi.org/10.1002/asl.878